Dynamics of polythiophene with defects

1991 J. Phys.: Condens. Matter 3 8803

(http://iopscience.iop.org/0953-8984/3/45/005)

J. Phys.: Condens. Matter 3 (1991) 8803–8824. Printed in the UK

Dynamics of polythiophene with defects

G Poussigue†, C Benoit†, J-L Sauvajol†, J-P Lere-Porte‡ and C Chorro‡

† Groupe de Dynamique des Phases Condensées, Unité de Recherche associée au CNRS n° 233, Université Montpellier II, Sciences et Techniques du Languedoc, Place E Bataillon 34095 Montpellier, Cédex 5, France

‡ Laboratoire de Chimie Générale, Université Montpellier II, Sciences et Techniques du Languedoc, Place E Bataillon 34095 Montpellier, Cédex 5, France

Received 17 April 1991, in final form 24 June 1991

Abstract. New infra-red and Raman experiments on undoped and doped polythiophene films, obtained in various synthesis conditions, are reported. The samples present a broad distribution of conjugation length. To explain all the observed spectra we develop a discrete force field model. Then, using this model and a new powerful computing process, the spectral moments method, we have been able to interpret practically all principal features observed: not only are the calculated frequencies very close to the experimental data but the intensities and the behaviour with conjugation length of the infra-red and Raman lines are in fair agreement for undoped and doped polythiophene. In particular, in infra-red, the emergence upon doping of four intense lines at 1032, 1117, 1203 and 1334 cm^{-1}, and other features less intense, and in isotropic Raman scattering the reduction of the intensity of all lines, are nicely reproduced. Taking into account our previous results obtained for the perfect chain it is possible to furnish a reasonable interpretation of the infra-red and Raman spectra of the polythiophene. In particular, the infra-red activity is very well represented with a simple tensor charge model without explicitly taking into account the fluctuation of the charge density.

1. Introduction

In an earlier paper (Poussigue and Benoit 1989), the dynamics of polythiophene were investigated through the properties of a perfect crystal model. The adjustment of the effective in-plane constants for the potential led to a very good fit of the calculated infra-red and Raman modes with the corresponding experimental data both for hydrogenated (PT) and deuterated (PTD) undoped polythiophene. This analysis also enabled the determination of other peak frequencies. These peaks are most probably due to the presence of defects (chemical for undoped compounds and topological for doped ones). The present work concerns the study of the spectra and models of doped and undoped polythiophene. In order to have a better understanding of the exact nature of such defects in PT, we have performed a new series of experiments under various conditions of synthesis and dedoping processes. For all samples, infra-red and Raman spectra have been recorded at different stages. In such a way we have obtained information concerning the evolution of spectra with the conjugation length and also with the proportion of doping compound.

0953-8984/91/458803 + 22 $03.50

With all these infra-red and Raman results it is possible to develop some theoretical models to explain the observed features: one model for the undoped polymer with a finite length and the possibility of a chemical β defect and one model for the doped PT with a finite length, the presence of a bipolaron and also the possibility of a chemical β defect.

2. Experimental data

2.1. Synthesis

Infra-red and Raman experiments have been performed on 20 films of polythiophene. These films have been electrochemically prepared using different monomers (thiophene, bithiophene) and various solvents (acetonitrile, benzonitrile, nitrobenzene, propylene carbonate). The synthesis has been made in the temperature range 5 °C–40 °C and under a variable amount of oxygen and water. The oxidized as-grown films were initially electrochemically reduced and then fully undoped by immersion in methanol. At the end of this treatment we used infra-red spectroscopy to control the amount of dopant; it was negligible and no chemical degradation could be attributed to this treatment.

The aim of this synthesis is to obtain polythiophene films which present a broad distribution of conjugation length (N_c). The N_c values were obtained from infra-red data by using the procedure given by Akimoto *et al* (1986). The order of magnitude of the conjugation length is derived from the ratio $R_{N_c} = I_{sym}/I_{anti}$ of the two infra-red lines assigned to the C=C symmetric stretching mode (1460–1417 cm^{-1} for the different oligomers) and to the antisymmetric stretching mode (1491 cm^{-1}) respectively. This ratio decreases monotonically but non-linearly as the number of thiophene rings increases (Akimoto *et al* 1986, Furukawa *et al* 1987). For our series of films R_{N_c} is in the range <0.3–1.5.

2.2. Infra-red and Raman spectra

Infra-red spectra were recorded using a Fourier transform spectrometer (BOMEM). The instrumental resolution was fixed at 4 cm^{-1}. The majority of the experiments have been performed at room temperature.

Raman spectra were recorded using a triple monochromator spectrometer (CODER 800). The instrument's linewidth was fixed at 7 cm^{-1}. The 5145 Å line of an argon ion laser was used as the light source. A back-scattering configuration was adopted. In order to avoid local heating and degradation of the film the light power was limited to below 5 mW and the incident beam was defocused. The majority of the experiments have been performed at low temperature: $T = 10$ K.

2.2.1. Neutral polythiophene: infra-red results. In figure 1 are displayed infra-red spectra obtained from three films of undoped polythiophene at room temperature. The conjugation length increases from the bottom to the top of the figure. The changes of the line positions in the infra-red spectra are relatively weak with regard to the distribution of the R_{N_c} values shown by the variation of the intensity lines ratio I_{sym}/I_{anti} (from 1.02 to 0.71). In fact we observe some variations of line intensity as the conjugation length increases: a large decrease of the broad 1439 cm^{-1} line, a slow decrease of the 1491 cm^{-1} line, relative stability of the 1356 cm^{-1} line (overlapped towards the low frequencies by

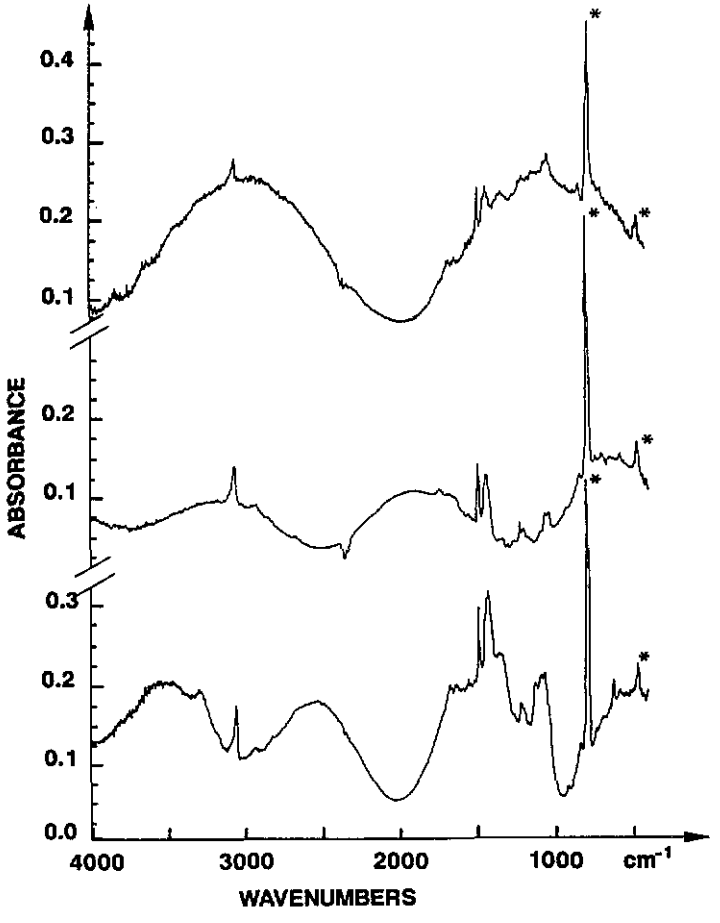

Figure 1. Infra-red spectrum for three samples of undoped PT. The conjugation length increases from the bottom to the top of the figure. * Lines corresponding to out-of-plane vibrational modes.

a line due to some traces of doped polymer) and always a predominance of the 785 cm^{-1} out-of-plane line. The triplet about 1050–1100 cm^{-1} in the bottom spectrum becomes a sharper peak near 1050 cm^{-1} in the top spectrum. Around 1200 cm^{-1} the situation is not so clear: there is a line at 1225 cm^{-1} and also some features due to some traces of doped polythiophene.

2.2.2. Neutral polythiophene: Raman results. In figure 2 are displayed Raman spectra obtained from five films of polythiophene at $T = 10$ K. The conjugation length increases from the bottom to the top of the figure. The changes of the Raman spectra are relatively weak with regard to the large distribution of the R_{N_c} values; nevertheless, significant modifications of the Raman spectrum can be analysed in relation to the different features of films under consideration. Some works have been devoted to the study of the sample dependence of the Raman spectrum of polythiophene (Akimoto *et al* 1986, Furukawa *et al* 1987, Yong and Renyuan 1985, Vardeny *et al* 1987, Sauvajol *et al* 1990). Our results

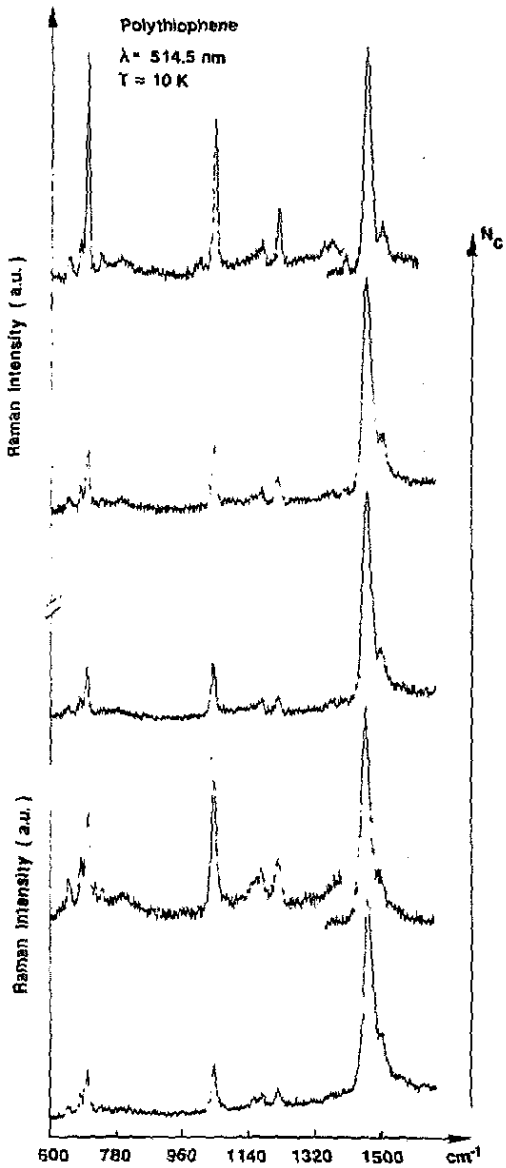

Figure 2. Raman spectrum for five samples of undoped PT. The conjugation length increases from the bottom to the top of the figure. The intensity scale is not the same in all parts of the spectra: the 1047 cm^{-1} line has almost the same intensity in all spectra.

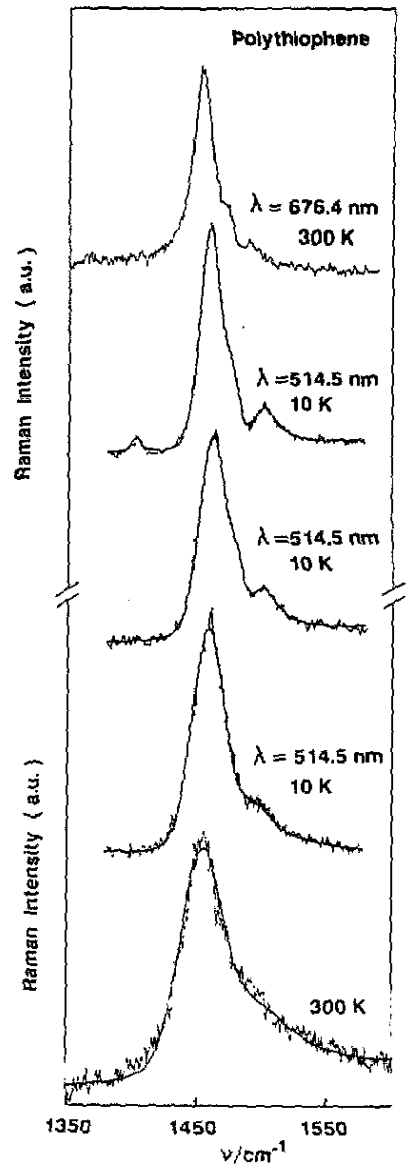

Figure 3. Detail of Raman spectrum around 1460 cm^{-1} for various samples of undoped PT. The conjugation length increases from the bottom to the top of the figure. The excitation line and the recording temperature are indicated on each spectrum. The two spectra at the top of the figure correspond to the same sample.

support the conclusions of these previous works. Here we report some new data supplied from our experiments.

First, we are interested in the wave-number region 600–1400 cm^{-1}. The Raman spectrum exhibits three strong lines at 700 cm^{-1}, 1047 cm^{-1} and 1222 cm^{-1} and these are

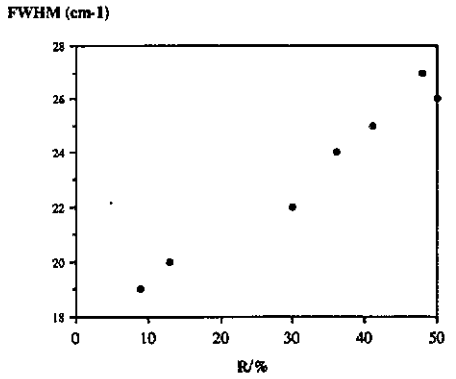

Figure 4. Full width at half height for the 1462 cm^{-1} PT Raman line against the ratio $R = I_{682}/I_{700}$.

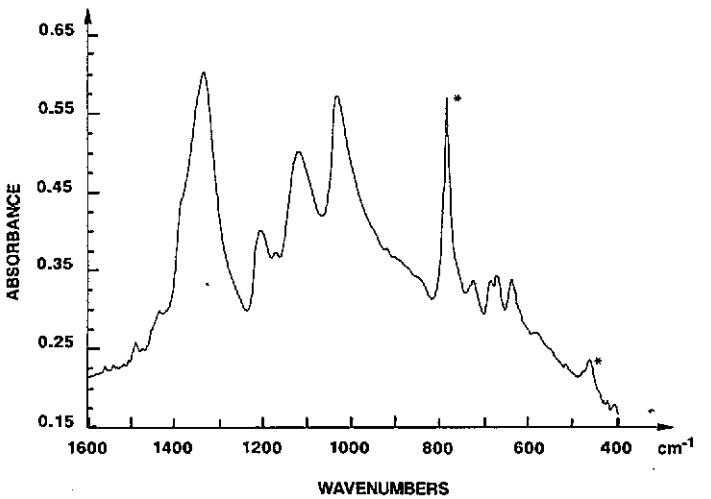

Figure 5. Part of the infra-red spectrum of a partially doped PT sample. * Indicates lines corresponding to out-of-plane vibrational modes.

currently assigned to the ring symmetric bending vibrational mode, to the in-plane C—H bending mode and to the C—C inter-ring stretching mode respectively. The intensities of some Raman lines (740 cm^{-1}, 791 cm^{-1}, 1000 cm^{-1}) increase with the conjugation length. They can be assigned to normal modes or to combination modes of the chain. Contrary to this behaviour, the intensity of other Raman lines (682 cm^{-1}, 723 cm^{-1}, 1455 cm^{-1}) decreases more or less strongly when N_c increases. They can be assigned to defects. In particular, the 682 cm^{-1} line is considered to be related to the distorted conformation around the inter-ring single bonds (Akimoto *et al* 1986, Furukawa *et al* 1987). The ratio between the intensity of this line and the intensity of the 700 cm^{-1} Raman line gives an evaluation of the amount of the distorted structure. A correlation between the decrease in the ratio $R = I_{682}/I_{700}$ and the decrease of R_{N_c} has been stated. That means that the conjugation length is strongly correlated with the abundance of coplanar segments.

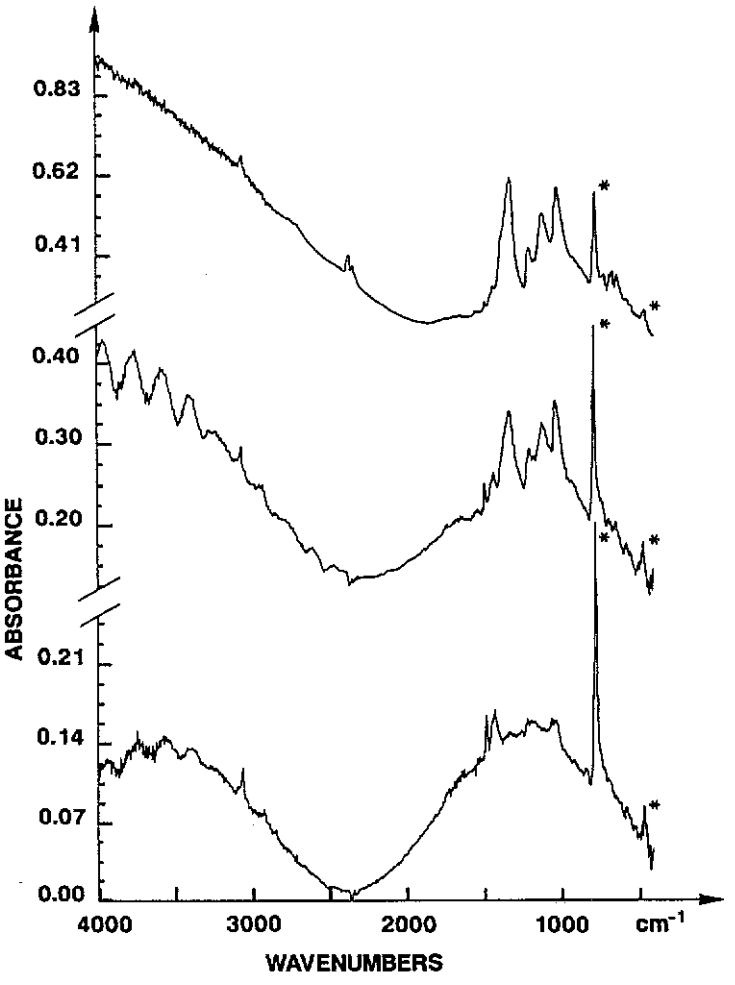

Figure 6. Evolution of the infra-red spectrum of a PT sample with dedoping (from top to bottom. * Indicates lines corresponding to out-of-plane vibrational modes.

The most striking features of our Raman data appear in the wave-number region around 1460 cm^{-1} (figure 3). When R decreases we observe: (i) the 1462 cm^{-1} C=C stretching mode narrows (figure 4); (ii) a Raman line at 1476 cm^{-1} emerges in the wing of the previous line; this line also appears for an exciting line in the red region; (iii) the profile of the 1500 cm^{-1} Raman line drastically changes: for small R (large N_c) it appears like a narrow peak—this peak does not disappear for an incident wavelength in the red region. When R increases (smaller N_c) a large broadening of the line occurs. Taking account of these behaviours, the 1462 cm^{-1}, 1476 cm^{-1} and 1500 cm^{-1} Raman lines have been assigned to normal modes of perfect polythiophene. We suggest that in the 1500 cm^{-1} region the normal mode (B_{2g} symmetry) of the chain overlaps with a defect mode, this latter mode becomes predominant when N_c decreases.

In summary, from a detailed analysis of the sample dependence of the Raman spectrum we have been able to assign the Raman lines related to the vibrational modes

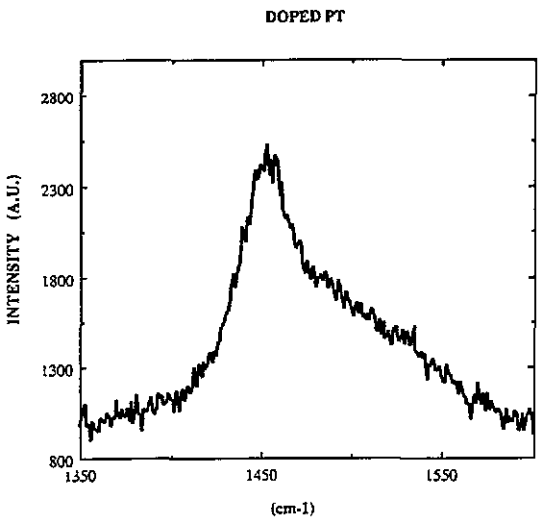

Figure 7. Detail of the Raman spectrum of a doped PT sample.

of the perfect (planar conformation and long conjugated segment) polythiophene chain. On the other hand, we have highlighted changes in Raman spectra in relation to the value of the conjugation length.

2.2.3. Doped polythiophene: infra-red results. Figure 5 exhibits a part of the infra-red spectrum of a partially doped PT sample after only one dedoping operation just after the synthesis. The most important fact is the emergence of four intense lines at 1032, 1117, 1203 and 1334 cm^{-1} which can be compared to the line at 784 cm^{-1} (out of plane mode) and are relatively stable from undoped to doped PT. Other features, less intense, can be found at 640, around 680 (doublet) and around 727 (doublet) cm^{-1}.

In figure 6 it is possible to see the evolution of the infra-red spectrum shown by three spectra of the same sample as in figure 5 recorded after some other successive dedoping operations (from the top to the bottom of the figure). The most important fact is the large decrease of intensities of the four main lines.

2.2.4. Doped polythiophene: Raman results. Upon doping, the intensity of all the Raman lines strongly decreases and more significant changes occur in the region around 1460 cm^{-1}: (i) the C=C stretching mode shifts to a lower frequency at 1455 cm^{-1} (ii) the 1500 cm^{-1} band exhibits a strong broadening and the relative intensity of this band increases (figure 7).

3. Models

To explain all the experimental details observed in the various spectra of PT, the crystal model of an infinite chain, as described by Poussigue and Benoit (1989), is not adequate. So, we have to make the basic assumptions somewhat more sophisticated, in order to reproduce numerically these features.

Table 1. Changes in the internal force constants. A: new values for three internal force constants. B: four new internal force constants (for H atoms at end chains in the α position). B_s stands for any external bisector; C_{ex} means that this carbon is in the next cycle.

A	
fC*=C, C*—S	= 0.283 mdyn Å^{-1}
fC=C, C—S	= −0.267 mdyn Å^{-1}
$f\angle B_s$—C*—C_{ex} $\angle$C—S—C*	= 0.214 mdyn Å rad^{-2}
B	
fC—H	= 5.250 mdyn Å^{-1}
$f\angle B_s$—C—H	= 0.940 mdyn Å^{-1}
fC*—S, $\angle B_s$—C*—H	= −0.230 mdyn rad^{-1}
$f\angle B_s$—C*—H $\angle$C—S—C*	= 0.010 mdyn Å rad^{-2}

* Indicates common atoms.

3.1. Crystal model

As can be found in Poussigue and Benoit (1989), the equilibrium configuration of the polymer is denoted by an infinite linear chain with a plane unit cell composed of two thienyl cycles head to tail. To study the in-plane modes, it is not necessary to take into account the in-space distribution of the parallel chains or the interchain force field.

The harmonic in-plane force constants fitted from the wave-numbers of the assigned peaks in the experimental infra-red and Raman spectra of PT and PTD are also given in this paper.

3.2. Model for the undoped PT

In this case it is satisfactory to alter the infinite chain to a finite one with two supplementary hydrogen atoms at the chain-ends. The equilibrium positions of the atoms are computed with the same values of interatomic distances and angles. For the two chain-end H atoms in α position we take r_{C-H} = 1.081 Å and $\angle$H—C=C = 124°.

For the harmonic force field, the values of the interatomic force constants are fixed to those obtained with the crystal model (except for three values which were fitted again in order to exchange two near isotropic Raman lines with contrasted intensities; their new values are given in table 1); this is done whatever the length of the chain. Such an assumption seems good for chains with at least two thienyl cycles. Only four supplementary force constants are needed for the two chain-end H atoms and their interactions; their values have been fixed according to thiophene ones; these constants are also given in table 1. This model is called UNDOP.

We have also tested, besides the finite character of the chain, the possibility of a chemical defect, i.e. the intercycle bond between two thienyl cycles in the β position for the two cycles. Such a defect gives two parallel parts for the chain. This model needs no supplementary constant for the harmonic force field. For the inter-ring bond in the β position we take r_{C-C} = 1.482 Å and $\angle$C—C=C = 122°. A part of the skeleton of such a polymer is drawn in figure 8(*a*). This model is called UNDOP1.

3.3. Model for the doped PT

To explain all the new features which appear in the various spectra of doped PT it is necessary to make the hypothesis that the doping process induces two transformations

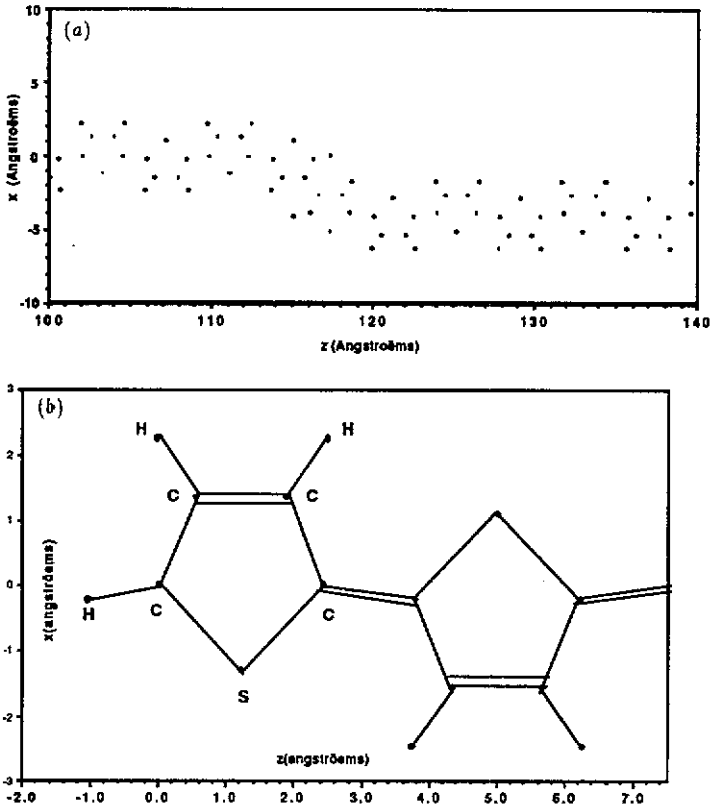

Figure 8. (*a*): PT chain with a parallel β defect. (*b*): Quinonic structure for PT.

on the chains of the polymer: the appearance of electric charges or holes (according to the character n or p of the doping compound) and, simultaneously, a topological modification in order to ensure the minimization of the total energy. The more stable configuration, which appears as the quantity of doping increases, corresponds to a double electric charge (or hole) on the chain and is associated with a local transformation (along a few thienyl cycles) of the aromatic configuration into a quinonic form. This phenomenon, known as a bipolaron, is numerically described with the equations developed by Brazovskii and Kirova (1981) and also by Onodera (1984). Three parameters entirely define this bipolaron: the position n° of its centre on the chain (facing a counterion), its linear extension I and its maximum amplitude A_{max}; these last two parameters are in fact derived from those L and ν of the formula giving the amplitude A of the bipolaron for a C atom in position n.

$$A_C(n) = \tanh(\nu) * \left(\tanh((n - n^\circ)/L + \nu/2) - \tanh((n - n^\circ)/L - \nu/2)\right)/2 \tag{3.1}$$

with

$$A_{max} = A_C(n^\circ) = \tanh(\nu) * \tanh(\nu/2) \tag{3.2}$$

and

$$I \approx L * (\nu + 2). \tag{3.3}$$

$A_C(n) = 0$ corresponds to the aromatic form; $A_C(n) = 1$ to the quinonic form.

For an S atom we take $A_S = (A_C(4p - 3) + A_C(4p))/2$ for the bipolaron amplitude; p is the number of the thienyl cycle containing the S atom.

The equilibrium distances and angles for the quinonic form are derived very simply from those of the aromatic one and are in agreement with the values calculated for the doped quaterthiophene by Bredas *et al* (1984). A part of the quinonic structure is shown in figure 8(*b*). For the internal force field we modify only the force constants corresponding to the stretching of C—C and C=C bonds, according to:

$$f_{(C-C)_{quin}} = (f_{(C-C)_{arom}} + f_{(C-Cex)_{arom}})/2 \tag{3.4}$$

$$f_{(C=C)_{quin}} = f_{(C=C)_{arom}} + \Delta \tag{3.5}$$

$$f_{(C=Cex)_{quin}} = f_{(C=C)_{arom}} - \Delta \tag{3.6}$$

with

$$\Delta = (f_{(C-C)_{arom}} - f_{(C-Cex)_{arom}})/2. \tag{3.7}$$

Along the chain, the positions of the atoms are computed taking into account the local values of the A deformation amplitudes through a linear interpolation between aromatic and quinonic values of the distances and angles. The same procedure is applied to calculate the effective force constants between carbon atoms along the chain. For the bending constant of the C—H group a correction, which is a maximum for $A = 0.5$, is also applied. This model is noted DOP. If we combine this bipolaronic model with a possible β defect we obtain a new model noted DOP1.

4. Calculation methods

4.1. Dynamical matrix

The dynamical matrix D is computed for

(i) finite chains of various lengths with H atoms at chain ends;
(ii) finite chains with a parallel β defect anywhere on the chain;
(iii) finite chains with a bipolaron centred anywhere on the chain;
(iv) finite chains with a parallel β defect and a bipolaron centred anywhere on the chain.

In all these cases the D matrix is derived in a compact form in order to use a minimum number of computer memories. It was possible to calculate D for polythiophene structures containing up to 100 elementary thienyl cycles with the help of a microcomputer.

4.2. Derivation of the infra-red and Raman spectra

It is well known that it is necessary to compute all eigenfrequencies and eigenvectors in order to compute the infra-red and Raman spectra. Here with the system being no more translation invariant, it is necessary to diagonalize directly the dynamical matrix. This presents some difficulties for large systems.

We use a new method based on the computation of the moments of the response of the system.

4.2.1. Infra-red. The infra-red absorption is directly related to the imaginary part $\bar{\bar{\chi}}''(q, \omega)$ (with $q \approx 0$) of the dielectric subsceptibility tensor. $\bar{\bar{\chi}}''(q, \omega)$ is correlated to the displacement–displacement correlation function. It is possible to show that for harmonic systems

$$\chi''_{\alpha\beta}(q \approx 0, \omega) = \sum_j c_\alpha(j) c^*_\beta(j)(\delta(\omega - \omega_j) - \delta(\omega + \omega_j))/2\omega_j \tag{4.1}$$

with

$$c_\alpha(j) = \sum_{n\varepsilon} q_{\alpha,\varepsilon}(n) e_j(n\varepsilon)(m_n)^{-1/2} \tag{4.2}$$

where ω_j and e_j are, respectively, the frequency and the polarization of the jth mode of vibration, $\bar{\bar{q}}(n)$ and m_n are the effective charge tensor and the mass of the nth atom.

4.2.2. Raman scattering. The time average of the power flux of the scattered light in a given direction, with a frequency between ω_f and $\omega_f + d\omega_f$ and within a solid angle $d\Omega$, is related to the differential scattering cross-section, which is given for unpolarized incident light by

$$d^2\sigma = \frac{1}{8\Pi^2 c^4} \omega_f^3 \omega_i [n(\omega) + 1]\hbar \sum_i \sum_{\alpha\gamma\beta\lambda} n^i_\alpha n^i_\beta I_{\alpha\gamma\beta\lambda} \bar{n}^k_\gamma \bar{n}^k_\lambda \, d\Omega \, d\omega_f \tag{4.3}$$

where

$$I_{\alpha\gamma\beta\lambda} = \sum_j a^*_{\alpha\gamma}(j) a_{\beta\lambda}(j) \frac{1}{2\omega_j} [\delta(\omega - \omega_j) - \delta(\omega + \omega_j)] \tag{4.4}$$

with

$$a_{\alpha\gamma}(j) = \sum_{n\varepsilon} \frac{\chi_{\alpha\gamma,\varepsilon}(n)}{\sqrt{m_n}} e_j(n\varepsilon) e^{iqr_n} \qquad q \approx 0 \tag{4.5}$$

where ω_i is the frequency of the incident light $\bar{n}^k$ $(k = 1, 2)$ and n^i $(i = 1, 2)$ are the polarization unit vectors for the incident and scattered light respectively; $\bar{n}^1$ (n^1) and $\bar{n}^2$ (n^2) are two mutually perpendicular unit vectors both perpendicular to the direction of propagation of the light, $n(\omega)$ is the Boltzmann factor, $\bar{\bar{\chi}}(n)$ is a third order tensor showing the fluctuation of the polarizability with the atomic motions. In the following we assume that the incident and scattered light are polarized parallel to the axes of the laboratory frame and then $\gamma = \lambda$, $\alpha = \beta$.

4.3. Spectral moments method

Essentially, the spectral moments method is based on a recursive technique like the ones initially developed by Lanczos (1950) to determine the eigenvalues of large matrices. These techniques have been largely used by Haydock (1980) in solid state physics to calculate the local density of electronic states of large clusters. When we apply these techniques to a dynamical system, it is possible to show (Benoit 1987) that the linear response (infra-red, Raman, neutron scattering, etc) is a projected density of one-phonon states. This result is of great importance. Furthermore, the method using the spectral moments is very stable, well-conditioned and more general than the Lanczos scheme.

Let us consider the following function

$$f(\omega) = \sum_j |c(j)|^2 \, (\delta(\omega - \omega_j) + \delta(\omega + \omega_j))/2\omega_j \tag{4.6}$$

where $c(j)$ is a vector with components

$$c_\alpha(j) = \sum_{n\varepsilon} q_{\alpha,\varepsilon}(n) e_j(n\varepsilon) (m_n)^{-1/2} \qquad \text{for infra-red}$$

or $c(j)$ is a tensor with components

$$c_{\alpha\beta}(j) = \sum_{n\varepsilon} \chi_{\alpha\beta,\varepsilon}(n) e_j(n\varepsilon) (m_n)^{-1/2} \qquad \text{for Raman scattering.}$$

We note that the form of $f(\omega)$ is identical (for $\omega > 0$) to every component of the infra-red response and to the Raman scattering cross-section for a given polarization of the incident and scattered lights. The constant and the Boltzmann factor are known and do not give any difficulties. So, a knowledge of $f(\omega)$ is sufficient for the knowledge of the response of the system. Since $f(\omega)$ is symmetrical in ω it can be written

$$g(u) = \sum_j |c_j|^2 \delta(u - \lambda_j) \tag{4.7}$$

with $u = \omega^2$ and $\lambda_j = \omega_j^2$.

To develop the spectral moments method (Benoit 1987, Benoit and Poussigue 1989) it is convenient to introduce the Dirac bracket formulation. In the representation $|n\varepsilon\rangle$

$$D_{n\varepsilon n'\varepsilon'} = \langle n\varepsilon | D | n'\varepsilon' \rangle \qquad e_j(n\varepsilon) = \langle n\varepsilon | j \rangle \qquad D|j\rangle = \lambda_j |j\rangle \tag{4.8}$$

and with

$$|v(q)\rangle = \sum_{n\varepsilon} v_{n\varepsilon}(q) (m_n)^{-1/2} |n\varepsilon\rangle \tag{4.9}$$

where $v_{n\varepsilon}(q)$ represents the 'charge' tensor ($q_{\alpha,\varepsilon}(n)$ or $\chi_{\alpha\beta,\varepsilon}(n)$) of the atom n.

$g(u)$ can be expressed as:

$$g(u) = \sum_j |\langle v(q) | j \rangle|^2 \, \delta(u - \lambda_j). \tag{4.10}$$

The nth moment of $g(u)$ is then given by

$$\mu_n = \int g(u) u^n \, \mathrm{d}u = \langle v(q) | D^n | v(q) \rangle. \tag{4.11}$$

So the determination of $g(u)$ can be directly carried out from matrix $\boldsymbol{D}$ without any diagonalization. However, the determination of $g(u)$ from moments μ_n is not easy and it is better to use generalized moments. It is possible to show that

$$g(u) = -(1/\pi) \lim_{\varepsilon \to 0_+} \left(\mathrm{Im}(R(z)) \right) \tag{4.12}$$

with

$$z = u + \mathrm{i}\varepsilon \, (\varepsilon \to 0_+) \qquad R(z) = \langle v(q) | (zI - \boldsymbol{D})^{-1} | v(q) \rangle.$$

The method consists of developing $R(z)$ in a continuous fraction

$$R(z) = b_0/(z - a_1 - b_1/z - a_2 - b_2/z - a_3 - b_3/\ldots) \tag{4.13}$$

and to calculate a_s and b_s from the elements of $\boldsymbol{D}$. One obtains the following relations

$$a_{s+1} = \tilde{\nu}_{ss}/\nu_{ss} \tag{4.14}$$

$$b_s = \nu_{ss}/\nu_{s-1s-1} \tag{4.15}$$

with

$$b_0 = \nu_{00} \tag{4.16}$$

where ν_{ss} and $\tilde{\nu}_{ss}$ are the spectral generalized moments, which are given by

$$\nu_{ss} = \langle v(\boldsymbol{q})|P_s(\boldsymbol{D})P_s(\boldsymbol{D})|v(\boldsymbol{q})\rangle \tag{4.17}$$

$$\tilde{\nu}_{ss} = \langle v(\boldsymbol{q})|P_s(\boldsymbol{D})\boldsymbol{D}P_s(\boldsymbol{D})|v(\boldsymbol{q})\rangle \tag{4.18}$$

where $P_s(u)$ are orthogonal polynomials which obey the recurrence relation

$$P_{s+1}(\boldsymbol{D}) = \boldsymbol{D}P_s(\boldsymbol{D}) - a_{s+1}P_s(\boldsymbol{D}) - b_sP_{s-1}(\boldsymbol{D}). \tag{4.19}$$

The coefficients a_s and b_s are calculated one after the other and hence $R(z)$ and $g(u)$ can be derived. The number of coefficients a_s and b_s needed is determined by the type of spectrum. For polythiophene spectra calculations this number is about 100.

4.4. Derivation of the one-phonon density spectrum

If we choose a normalized random number for the 'charges' $v_{n\varepsilon}(q)$ in equation (4.9), it can be shown (Benoit *et al* 1991) that the spectrum derived by the application of the spectral moments method is almost exactly the one-phonon density spectrum; the fit of these two spectra is as good as the dimension of the dynamic matrix is large. For dimensions of a few hundreds it is necessary to calculate several spectra with different choices of the random 'charges' and then take the averaged spectra.

5. Numerical results against experimental data

5.1. Neutral polythiophene

5.1.1. Infra-red and Raman spectra for the UNDOP *model.* These various spectra have been computed for different values of the chain length which itself is equal to the conjugation length in this simple model. These spectra are reproduced in figures 9(*a*) and 10(*a*) respectively for infra-red and isotropic Raman spectra. In the infra-red case we give the total calculated spectrum for four lengths of the chain (2, 6, 24, 40 thienyl cycles). In the Raman case we give the calculated spectrum for three lengths of the chain (6, 24, 40 thienyl cycles).

In table 2 we give the roughly adjusted values of the effective atomic electric tensor charges used to compute the total infra-red spectra (as the sum of polarized components) and the values of the effective atomic susceptibility derivatives used to compute the isotropic Raman spectra.

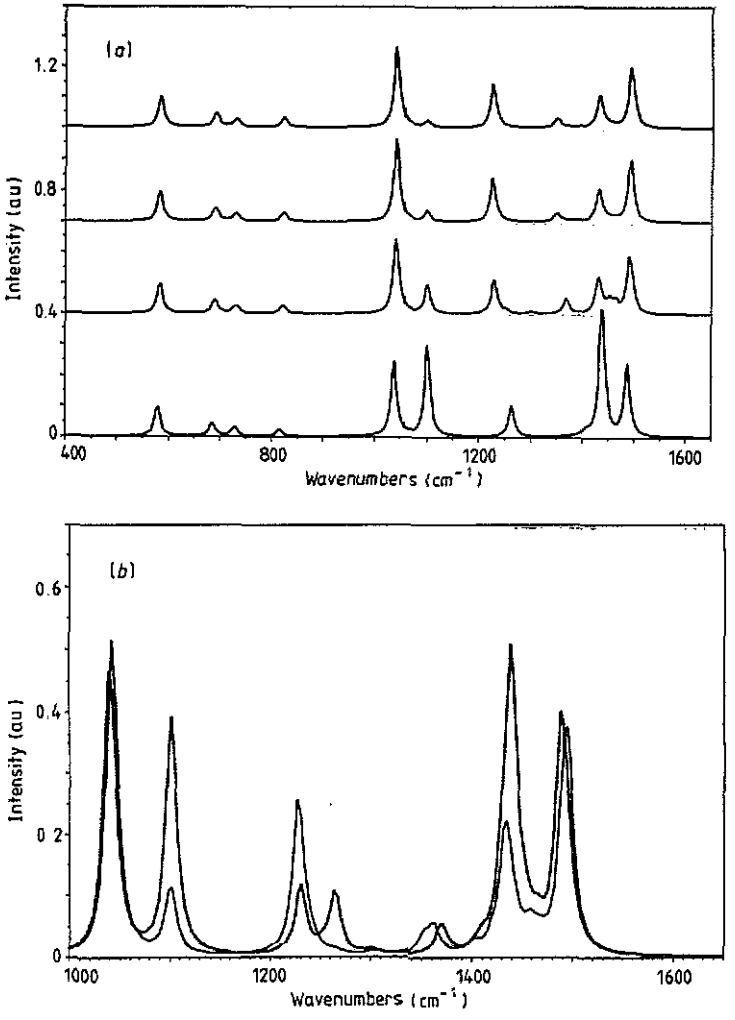

Figure 9. (*a*) Four PT calculated total infra-red spectra for the UNDOP model. From the bottom to the top, they correspond respectively to a chain of 2, 6, 24, 40 thienyl cycles. (*b*) Realistic PT calculated total infra-red spectra for the UNDOP model. The full curve corresponds to a high conjugation mixing (chains of 24 and 8 thienyl cycles). The broken curve corresponds to a low conjugation mixing (chains of 6 and 2 thienyl cycles).

5.1.2. Infra-red spectra for the UNDOP1 model. These spectra have been computed for different values of the total length of the chain and different positions for the β defect. The conjugation length in this case is equal to the length of the largest part of the chain. The electric charges are the same as for the UNDOP model. In order to show the calculated effect of the β defect, the graph in figure 11(*a*) represents the difference between two calculated spectra: one for the UNDOP1 model, with 30 thienyl cycles for the left part and 10 thienyl cycles for the right part, and one for the UNDOP model with 40 thienyl cycles.

5.1.3. Comparison with experimental features. For the infra-red spectra, if we compare the experimental plots of figure 1 to the calculated ones of figures 9(*a*), 9(*b*) and 11 (*a*),

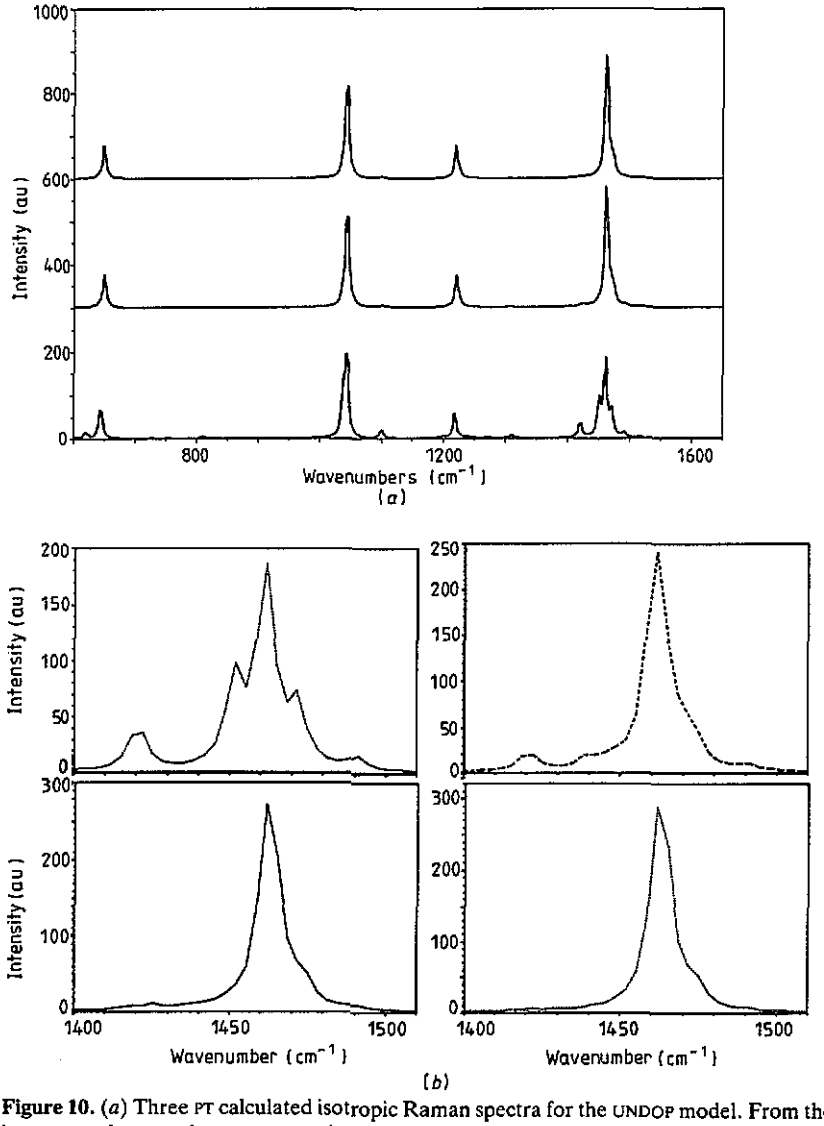

Figure 10. (*a*) Three PT calculated isotropic Raman spectra for the UNDOP model. From the bottom to the top, they correspond respectively to a chain of 6, 24, 40 thienyl cycles. (*b*) Evolution of the PT calculated isotropic Raman spectrum with the conjugation length for the UNDOP model in the 1400–1500 cm^{-1} region. -----, ———, —— and ·····, respectively correspond to a chain of 6, 10, 20 and 40 thienyl cycles.

we can observe that the features described in section 2.2.1 and their evolution with the conjugation length are nicely reproduced. For example the large decrease of the line around 1450 cm^{-1} and the slow decrease of the 1491 cm^{-1} line with increasing conjugation length are shown in figure 9(*b*) which compares two spectra: one for PT with high conjugation (mixing of 8 and 24 thienyl cycles chains) and one for PT with low conjugation (mixing of 2 and 6 thienyl cycles chains). The triplet observed near 1100 cm^{-1} in the bottom spectrum of figure 1 can also be explained by the short conjugation length

Table 2. Effective atomic charges and atomic susceptibilities. A: effective atomic charges for the model with, for any atom i, $(\mu_z)_i = q_{si}z_i + q_{ti}x_i$ and $(\mu_x)_i = -q_{ti}z_i + q_{ti}x_i$; values take into account the symmetry properties $\varepsilon = \pm 1$ for atoms outside/inside the two sulphur atoms in a unit cell. B: effective atomic polarizabilities for isotropic Raman scattering taking into account the symmetry properties, $\varepsilon = \pm 1$, $\varepsilon' = \pm 1$ according to the position of the atom in a unit cell (along z and x axes) in arbitrary units.

		Aromatic form		Quinonic form	
	Atom type	q_{si} (electrons charge units)	q_{ti}	q_{si} (electrons charge units)	q_{ti}
A	C_α	−0.0115	0.0088ε	−0.0915	0.0088ε
	C_β	−0.1399	0.0052ε	−0.0599	0.0052ε
	H_β	0.0600	0.0167ε	0.0600	0.0167ε
	S	0.1828		0.1828	
	H_α (chain end)	0.0800		0.1600	
	C_α (chain end)	−0.0915		−0.1725	
B	C_α	1.2ε	$-2.6\varepsilon'$	-1.2ε	$3.0\varepsilon'$
	C_β	-1.2ε	$3.0\varepsilon'$	1.2ε	$-2.6\varepsilon'$
	H_β	0.5ε	$-0.3\varepsilon'$	0.5ε	$-0.3\varepsilon'$
	S		$2.0\varepsilon'$		$2.0\varepsilon'$
	H_α (chain end)		$-0.3\varepsilon'$		$-0.3\varepsilon'$
	C_α (chain end)	1.2ε	$-2.6\varepsilon'$	-1.2ε	$3.0\varepsilon'$

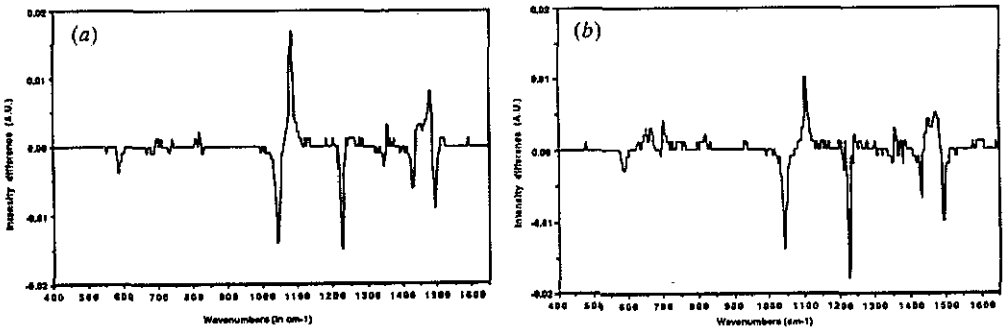

Figure 11. (*a*): difference between undoped PT calculated total infra-red spectra for the UNDOP1 model (parallel β defect, with 30 thienyl cycles for the left part and 10 for the right one) and for the UNDOP model (40 thienyl cycles chain). (*b*): difference between doped PT calculated total infra-red spectra for the DOP1 model (parallel β defect, with 30 thienyl cycles for the left part and 10 for the right one, bipolaron entirely localized in the left part) and for the DOP model (40 thienyl cycles chain with a bipolaron).

(bottom of figure 9(*a*) or figure 9(*b*)) and by a β defect (figure 11(*a*)). In the low frequencies region the out-of-plane lines are, of course, not reproduced by our in-plane model and the other lines are calculated with an intensity a little greater than the observed ones, this is probably due to our very simple model of effective charge tensors carried by the atoms.

For the Raman spectra, the main lines of the spectra of figure 2 and their evolution with increasing conjugation length are well reproduced by the calculated isotropic

Table 3. Bipolaron parameters.

	Present work	Bertho *et al* (1988) (pinned bipolaron case)
$n°$ (centre of bipolaron)	At chain middle	At chain middle
L	1.4 thienyl cycles	1.4 thienyl cycles
$D = \nu L$	5.95 thienyl cycles	4 thienyl cycles
$l = D + 2L$ (bipolaron length)	8.75 thienyl cycles	6.8 thienyl cycles
A_{max} (maximum amplitude)	97.5% $\tanh(\nu/2)\tanh(\nu)$	89% $\tanh(\nu/2)$

Raman spectra of figure 10(*a*). The only remaining problem from the observations of section 2.2.2 is the observed peak at 700 cm^{-1}: we think that this can be assigned to an out-of-plane cycle bending normal mode, the 652 cm^{-1} weak peak being assigned to an in-plane normal mode. Concerning the region around 1450–1500 cm^{-1} the experimental details shown in figures 3 and 4 are perfectly reproduced by the theoretical predictions as shown in figure 10(*b*) which gives the evolution of the Raman spectra with the conjugation length in the 1400–1500 cm^{-1} region.

5.2. *Doped polythiophene*

5.2.1. Determination of the bipolaron parameters for the DOP *model.* The three parameters which entirely define the bipolaron are $n°$, l and A_{max} (section 3.3) which are roughly adjusted in order to fit the doped PT spectra. They are reproduced in table 3 where they are compared with the values obtained by Bertho *et al* (1988) in electronic calculations.

5.2.2. Infra-red, Raman and one-phonon density of states spectra for the DOP *model.* These various spectra have been computed for different values of the length of the chain. They are shown in figures 12(*a*), 13(*a*) and 14 respectively for infra-red, Raman and one-phonon DOS spectra. In the infra-red case we give the calculated spectrum for four lengths of the chain (6, 8, 24, 40 thienyl cycles). In the Raman case we give the calculated spectrum for three lengths of the chain (6, 24, 40 thienyl cycles) and for the DOS for only one length (24 thienyl cycles).

In table 2 are also given the values taken for the effective atomic electric charges (the values obtained by Bredas *et al* (1984) in the doped quaterthiophene were a good starting point) and for the effective atomic susceptibility derivatives in the quinonic form. For each effective atomic quantity the local value of the deformation amplitude A is taken into account through a linear interpolation between aromatic and quinonic atomic quantities; moreover for the infra-red spectra a total charge opposite to the counterion charge is introduced which is displayed according to A values.

5.2.3. Infra-red spectra for the DOP1 *model.* These spectra have been computed for different values of the total length of the chain and different positions for the β defect. In order to show the calculated effect of the β defect on a doped polymer (essentially a line near 1110 cm^{-1}), figure 11(*b*) represents the difference between two calculated spectra: one for the DOP1 model, with 30 thienyl cycles for the left part and 10 thienyl

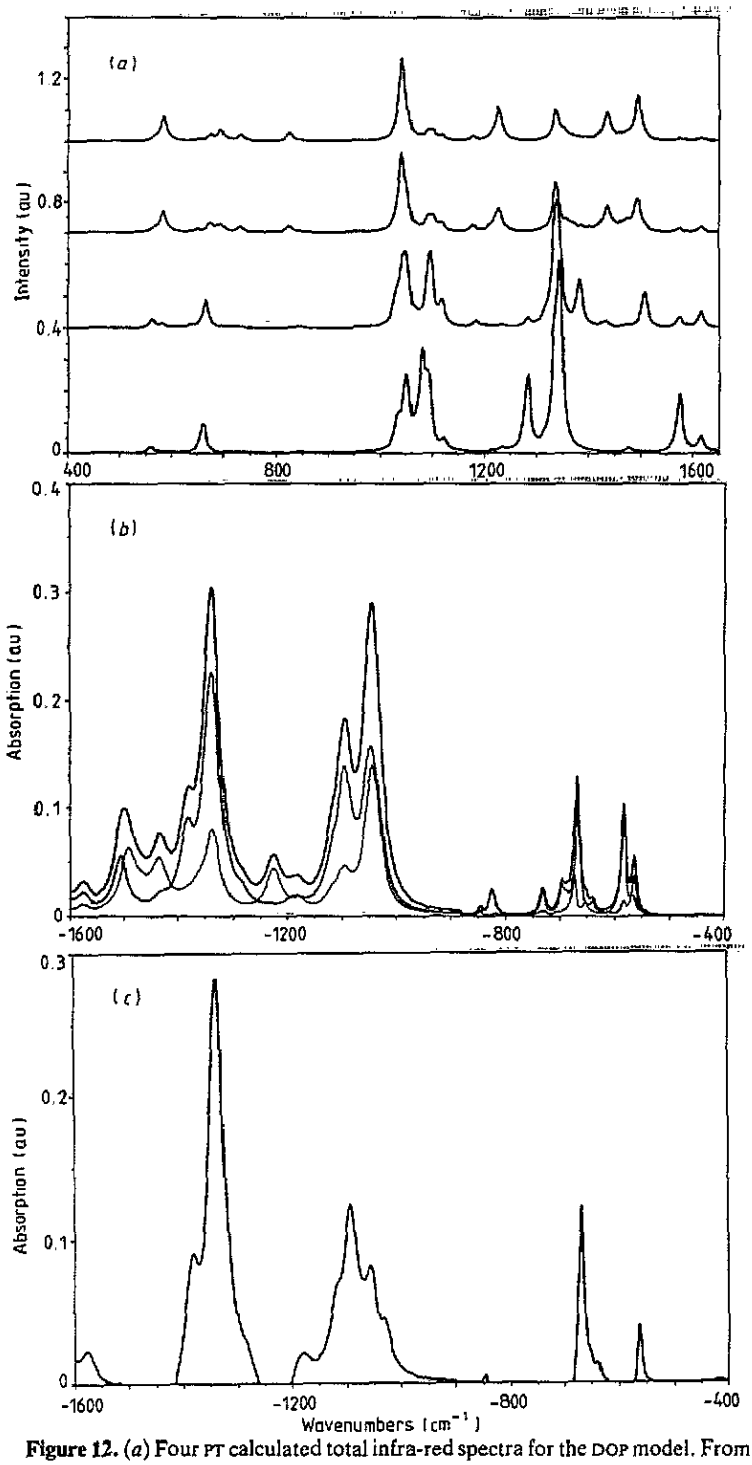

Figure 12. (*a*) Four PT calculated total infra-red spectra for the DOP model. From the bottom to the top, they correspond respectively to a chain of 6, 8, 24, 40 thienyl cycles. (*b*) The bold curve: realistic PT calculated total infra-red spectrum for the DOP model corresponding to a high conjugation mixing (chains of 24 and 8 thienyl cycles). The full curve corresponds to the 24 thienyl cycles chain. The broken curve corresponds to the 8 thienyl cycles chain. (*c*) Contribution of the bipolaron (DOP–UNDOP) to the realistic PT calculated total infra-red spectrum for high conjugation mixing (chains of 24 and 8 thienyl cycles).

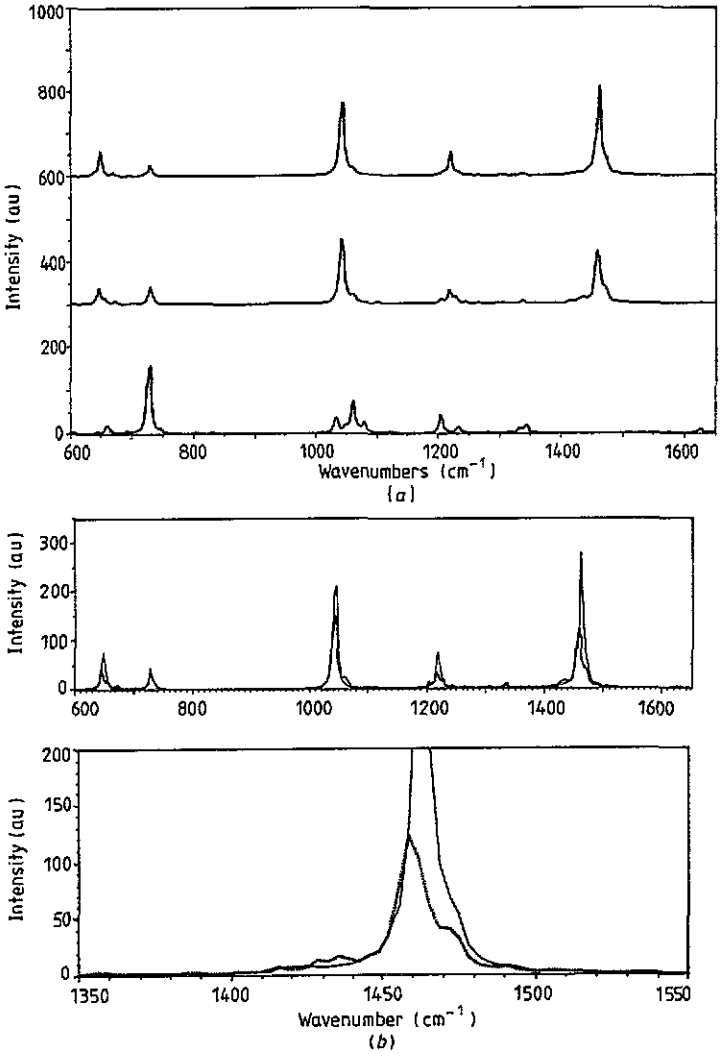

Figure 13. (*a*) Three PT calculated isotropic Raman spectra for the DOP model. From the bottom to the top, they correspond respectively to a chain of 6, 24, 40 thienyl cycles. (*b*) Top: comparison of PT calculated isotropic Raman spectra for the DOP and UNDOP models with a chain of 24 thienyl cycles. Bottom: detail of the 1350–1550 cm^{-1} region. The full curve corresponds to the undoped PT and the broken curve corresponds to the doped one.

cycles for the right part (the bipolaron is entirely in the left part), and one for the DOP model with 40 thienyl cycles.

5.2.4. Comparison with experimental features. For the infra-red data, if we compare the experimental spectrum of figure 5, which corresponds to a doped PT, with a rather good mean conjugation length, to the realistic calculated spectrum of figure 12(*b*) (mixing of 8 and 24 thienyl cycles chains with a bipolaron) we can observe that the features described in section 2.2.3 are satisfactorily reproduced especially in the region 1000–1500 cm^{-1} which corresponds to the four strong bipolaronic lines. The contribution of a β defect, as shown in figure 11(*b*), can broaden and shift towards 1110 cm^{-1}, the 1094 cm^{-1} line.

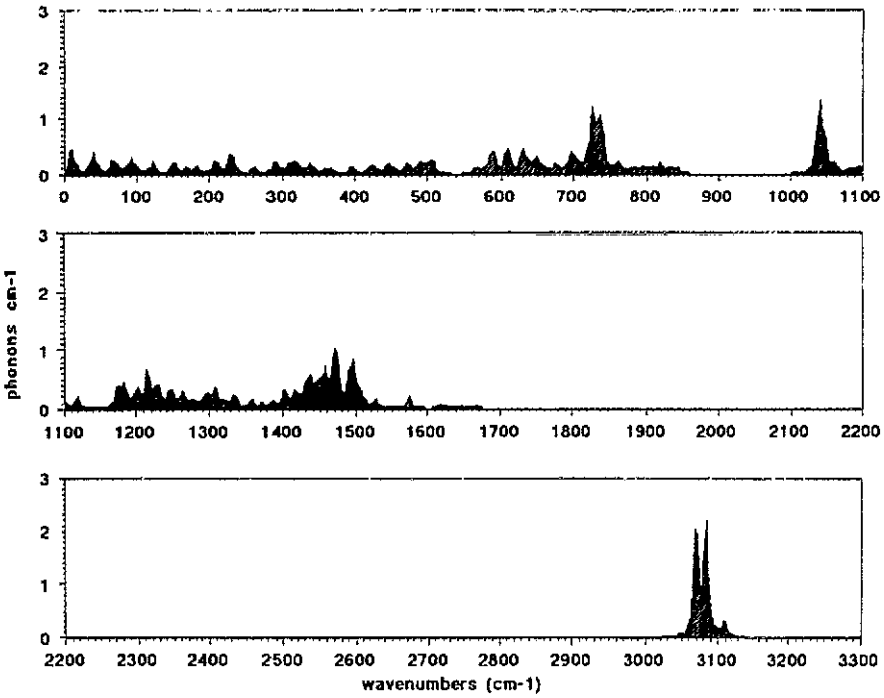

Figure 14. PT one-phonon density of states (in plane) for a 24 thienyl cycles chain in the DOP model.

Figure 12(*c*) explicitly gives the contribution of the bipolaron to the spectrum plotted in figure 12(*b*). It is easy to recognize in these figures the so called *T* modes (strong) and *R* modes (weak) (Heeger *et al* 1988) observed either in the photoinduced IRAV spectrum of PT (Moraes *et al* 1984, Schaffer and Heeger 1986) or in the doping induced IRAV spectrum (Hotta *et al* 1984, 1985, Hayes *et al* 1985 and also present work (figure 5)). Table 4 shows the comparison between observed IRAV lines and present calculated ones.

For the Raman data, if we compare the experimental detail of figure 7 with the calculated part of the spectrum shown in the bottom of figure 13(*b*) we can see the shift of the line towards a lower frequency at 1455 cm^{-1} and also the broadening near 1500 cm^{-1}. The spectra shown at the top of figure 13(*b*) illustrates the decrease of the Raman spectrum with doping as observed experimentally.

6. Conclusion

In this paper we have reported new infra-red and Raman experiments on undoped and doped polythiophene films which present a broad distribution of conjugation length. Our experimental results are in agreement with the results previous obtained by other authors. They interpreted their data in the frame of amplitude mode formalism (Horovitz 1982), or derived models (Lopez Navarrete and Zerbi 1991), which considers the coupling of phonons to electronic excitations (see Benoit *et al* 1990 for a review on this subject). Only phonons that modulate the amplitude of the order parameter couple to

Table 4. Calculated and observed infra-red lines in doped polythiophene. Data from doping induced IRAV spectrum: (*a*) Hotta *et al* (1984, 1985), (*b*) Hayes *et al* (1985). Data from photoinduced IRAV spectrum: (*c*) Moraes *et al* (1984), (*d*) Schaffer and Heeger (1986). Results from the crystal model: (*e*) Poussigue and Benoit (1989).

Intensity	Experimental wave-number Previous works cm^{-1}	Present work cm^{-1}	Calculated wave-number	Assignment
M		465	—	out of plane mode(*e*)
W		515	—	modes combination(*e*)
VW		555	564	bipolaron induced mode
W		583	584	in plane mode
M	640(*a*, *b*)	640	640	bipolaron induced mode
M	680(*a*, *b*)	675	668	(bip. ind. + in pl. short ch.) modes
M	690(*c*, *d*)	687	695	in plane long chains modes
VW		714	—	out of plane mode(*e*)
M	728(*c*, *d*) 730(*a*, *b*)	725–732	731	(in pl. + long ch. bip. ind.) modes
VS	782(*c*, *d*)	784	—	out of plane mode
VW		825	825	in plane mode
W		845	845	bipolaron induced mode
VW	900(*c*, *d*)	910	—	?
VS	1020(*a*, *b*, *c*, *d*)	1032	1044	(in plane + bip. ind.) modes
S	1120(*a*, *b*, *c*, *d*)	1117	1094	bipolaron induced mode
			1105	β defect induced mode
			1110	in plane chain end mode
W		1170	1185	bipolaron induced mode
M	1200(*a*, *b*, *c*, *d*)	1203	1226	(bip. ind. + in pl. long ch.) modes
VS	1323(*a*, *b*, *c*, *d*)	1334	1338	bipolaron induced mode
W		1380	1379	(in plane + bip. ind.) modes
W	1435	1430	1434	in plane short chains modes
VW		1470	1470	β defect induced mode
W		1489	1498	in plane modes
VW		1507	—	modes combination(*e*)
VW		1530	—	modes combination(*e*)
VW		1555	—	modes combination(*e*)
VW		1580	1576	bipolaron induced mode

the electronic density. Within the amplitude mode formalism there is one localized phonon for every Raman line of the pure polymer. They interpreted the observed strong infra-red modes (see table 4) as *T* modes which are consistent with the principal Raman lines. The other, weaker, lines are interpreted as 'ring lines' (Schaffer and Heeger 1986). Our model is a discrete force field model where the electron–phonon coupling is not explicitly taken into account, although the presence of the bipolaron under doping or photoexcitation is directly related to such coupling.

Then, using this simple model and a new computing method we were able to interpret practically all the principal features observed: not only are the calculated frequencies in agreement with the experimental data but the intensity and the behaviour of the infra-red and Raman lines are well reproduced for undoped and doped polythiophene. Let us summarize: for the undoped polythiophene, in infra-red, there is a large decrease of the broad line around 1440–1450 cm^{-1} with increasing conjugation length, a slow decrease of the 1491 cm^{-1} line and also a triplet about 1050–1100 cm^{-1}, which becomes a sharper peak near 1050 cm^{-1}. In Raman scattering we explained the narrowing of the

1462 cm^{-1} C=C stretching mode and the emergence of a line at 1476 cm^{-1} in the wing. Finally, for doped polythiophene, in infra-red, the emergence of four intense lines at 1032, 1117, 1203 and 1334 cm^{-1} and other features, less intense, found at 640, around 680 (doublet) and around 727 (doublet) cm^{-1} are well explained by our model. Likewise in isotropic Raman scattering, the decrease of the intensity of all lines upon doping, the C=C stretching mode shifting towards a lower frequency and the broadening of the 1500 cm^{-1} band with a relative increase of its intensity are explained.

Taking into account the previous results obtained for the perfect chain we were able to furnish a reasonable interpretation of the infra-red and Raman spectra of this material. It is clear that, for polythiophene, it is possible to represent very well the infra-red activity with a simple tensor charge model without explicitly taking into account the fluctuation of the charge density.

References

Akimoto M, Furukawa Y, Takeuchi H, Harada I, Soma Y and Soma M 1986 *Synth. Met.* **15** 353–360
Benoit C 1987 *J. Phys. C: Solid State Phys.* **20** 765–789
Benoit C, Rolland M and Palpacuer M 1990 *Phys. Status Solidi* b **162** 9–60
Benoit C and Poussigue G 1989 *High Performance Computing* ed J L Delaye and E Gelembe (Amsterdam: Elsevier) 347–56
Benoit C, Royer E and Poussigue G 1991 *J. Phys.: Condens. Matter* submitted
Bertho D, Laghdir A and Jouanin C 1988 *Phys. Rev.* B **38** 12531–9
Brazovskii S A and Kirova N N 1981 *Pis. Zh. Eksp. Teor. Fitz.* **33** 6–10
Bredas J-L, Thémens B, Fripiat J-G, André J-M and Chance R R 1984 *Phys. Rev.* B **29** 6761–73
Furukawa Y, Akimoto M and Harada I 1987 *Synth. Met.* **18** 151–6
Haydock R 1980 *Solid State Physics* vol 35, ed H Ehrenreich, F Seitz and D Turnbull (New York: Academic)
Hayes W, Pratt F L, Wong K S, Kaneto K and Yoshino K 1985 *J. Phys. C: Solid State Phys.* **18** L555
Heeger A J, Kivelson S, Schrieffer J R and Su W-P 1988 *Rev. Mod. Phys.* **60** 781–850
Horovitz B 1982 *Solid State Commun.* **41** 729
Hotta S, Shimotsuma W and Taketani M 1984 *Synth. Met.* **10** 85
Hotta S, Shimotsuma W, Taketani M and Kohiki S 1985 *Synth. Met.* **11** 139
Lanczos C 1950 *J. Res. NBS* **45** 255
Lopez Navarrete J T and Zerbi G 1991 *J. Chem. Phys.* **94** 957–64, 965–70
Moraes F, Schaffer H E, Kobayashi M, Heeger A J and Wuld F 1984 *Phys. Rev.* B **30** 2948
Onodera Y 1984 *Phys. Rev.* B **30** 775–85
Poussigue G and Benoit C 1989 *J. Phys.: Condens. Matter* **1** 9547–60
Sauvajol J-L, Chenouni D, Lere-Porte J-P, Chorro C, Moukala B and Petrissans J 1990 *Synth. Met.* **38** 1–12
Schaffer H E and Heeger A J 1986 *Solid State Commun.* **59** 415–21
Vardeny Z, Ehrenfreund E, Brafman O, Hegger A J and Wulf F 1987 *Synth. Met.* **18** 183–8
Yong Y and Renyuan Q 1985 *Solid State Commun.* **54** 211